GENERATION OF INITIAL FIBER ORIENTATION STATES FOR LONG FIBER REINFORCED THERMOPLASTIC COMPRESSION MOLDING SIMULATION

Louis Schreyer[a], Juliane Blarr[b], Katja Höger[c], Nils Meyer[a], Luise Kärger[a]

a: Institute of Vehicle System Technology, Karlsruhe Institute of Technology, Karlsruhe, Germany; louis.schreyer@kit.edu
b: Institute for Applied Materials - Materials Science and Engineering IAM-WK, Karlsruhe Institute of Technology, Karlsruhe, Germany
c: wbk Institute of Production Science, Karlsruhe Institute of Technology, Karlsruhe, Germany

Abstract: *The prediction of the fiber orientation state (FOS) is of utmost interest for compression molded long fiber reinforced thermoplastics as the part's properties strongly depend on it. Besides the position of the initial plastificate in the mold cavity and the process settings, detailed knowledge of the initial FOS is essential. During compounding, the fibers align depending on the extruder screw configuration yielding a non-uniform local FOS. For process simulation, a common approach is to neglect this effect and assume an isotropic or planar-isotropic FOS of the initial plastificate. A more sophisticated approach consists of micro-computed tomography (μCT-) scans of slices of the initial plastificate and the derivation of the initial FOS from the three-dimensional image data. This approach can yield accurate predictions but is quite cumbersome and expensive. In this paper, we present a novel approach to account for the FOS of the initial plastificate. The approach is motivated by experimental observations and based on geometric assumptions. Depending on the extruder type and the dimensions of the initial plastificate, the developed tool generates a three-dimensional data set containing the mesh information alongside the initial FOS in a tensorial representation. To investigate the influence of the initial FOS for different flow regimes, we conducted compression molding simulations on a planar part.*

Keywords: thermoplastic; compression molding; fiber orientation; plastificate; process simulation

1. Introduction

Compression molded long fiber reinforced thermoplastics (LFT) are widely used for large semi-structural parts in the automotive and aerospace industry. The main advantage of compression molded LFT compared to injection molded LFT is the final part's longer average fiber length due to lower shear forces during processing [1]. Its popularity increased with the introduction of the direct LFT in-line compounding (D-LFT-ILC) process, which offers additional degrees of freedom. Instead of semi-finished LFT pellets, thermoplastic granulate, additives and fibers are compounded in-line, reducing the supply chain. In the D-LFT-ILC process, the thermoplastic granulate and the additives are fed via a hopper to the first extruder, where they mix, and the thermoplastic material melts. In the second extruder (single or double screw extruder), fiber rovings are then fed continuously. Due to the shear forces introduced by the extruder screw(s), the fibers break and disperse, yielding a non-uniform local FOS. The compound is extruded into a predetermined shape via a nozzle and cut. When using a double screw extruder, the general fiber orientation of the plastificate resembles two swirls [2]. However, the fibers align in extrusion direction in the outermost layer. Finally, the extruded plastificate is transferred to a compression molding press and compressed into shape.

  doi:10.5075/epfl-298799_978-2-9701614-0-0

To predict a LFT part's mechanical properties accurately, the local FOS must be considered. Further, the FOS critically influences the part's dimensional stability. Therefore, detailed knowledge of the initial FOS in the plastificate and the reorientation phenomena during molding are of utmost interest, with this work focusing on the former. The FOS can be expressed in form of a probability density function $\psi(\cdot)$ [3]. A more convenient and computationally efficient tensorial representation based on moments of the probability density function was introduced by Advani and Tucker [4]. The second-order fiber orientation tensor (FOT) is defined as:

$$\boldsymbol{A} = \oint \boldsymbol{p} \otimes \boldsymbol{p} \psi(\mathbf{p}) \mathrm{d}\mathbf{p} \,. \tag{1}$$

$\boldsymbol{p}$ denotes the unit vector characterizing the direction of a single fiber and $\otimes$ denotes the outer product. Non-destructive methods to determine the local FOS are micro-computed tomography (µCT) [5-7] and terahertz spectroscopy [8], where the latter is only suitable for thin cross-sections (therefore not applicable for LFT plastificates). A general challenge with µCT scans depicts the conflict between the scan resolution and the sample size. With increasing scan resolution, the permissible sample size decreases and vice versa. This effect especially applies to carbon fibers (CF) due to their small diameter (5 – 7 µm). Further, the contrast between CF and thermoplastics is unpronounced on µCT images, due to their respective molecular structures. As a result, meaningful µCT scans of larger volumes (especially for CF) are time-consuming and storage-intensive. To partially circumvent this problem, at least for glass fibers (GF), Perez et al. [2] assumed that fiber bundles describe the local FOS in GF plastificates adequately, allowing a scan resolution lower than the diameter of the fiber (> 15 µm). The latter requires that the individual fibers stay in bundle-like configurations during compounding, which must be resolved by the µCT scan. A comparison by Perez et al. [2] with the FOS results from high-resolution scans (4 µm/voxel) at sample locations showed an average relative deviation of 23 percent when using VGStudio Max software to determine the FOS. Song et al. [9] additionally assumed periodicity of the FOS in the extrusion direction due to the nature of the flow. Further, they scanned a plastificate with a smaller cross-section (resolution: 50 µm/voxel) and mapped the FOS onto the simulated plastificate mesh. The simulation results showed the best agreement with the investigated GF reinforced LFT part's final FOS at sample locations compared to an isotropic and planar-isotropic initial FOS. In a later work, Song et al. [10] applied the latter workflow with an identical scan resolution to a CF plastificate (from a single screw extruder). The scanned volume was divided into (1 x 1 x 1) mm cells to determine the local FOS, corresponding to only (20 x 20 x 20) voxels per cell. However, the detection of CF bundles is unlikely due to the low resolution and the mentioned difficulties that arise in µCT scans with CF. The postprocessing algorithm more likely examines the FOS based on the local orientation of the matrix material. Nevertheless, the authors achieved good agreement with the experimental results. However, the good agreement is probably due to the simpler initial FOS caused by the used single screw extruder.

This work focuses on developing a novel method to consider the FOS of an LFT plastificate in compression molding simulations. The method approximates the averaged expected FOS based on the geometric construction of artificial fiber vectors (FV) rather than the local FOS, which is subjected to statistical variations. We compare the FOS from the plastificate generator with those from µCT scans qualitatively at selected locations. The influence of the initial FOS is discussed based on compression molding simulations for different initial FOS and flow regimes.

  doi:10.5075/epfl-298799_978-2-9701614-0-0

The investigated D-LFT-ILC plastificate was manufactured using a double screw extruder with the same direction of rotation and a (75 x 35) mm rectangular nozzle. The material of the investigated plastificate was 25 vol.% carbon fiber reinforced polyamide 6 (PA6).

2. Methods

2.1 Plastificate generator

The plastificate generator generates a three-dimensional data set (VTK file) containing the mesh information alongside the second-order FOT as cell data. The method was implemented in Python 3.8. An ideal plastificate is assumed with the cross-section dimensions of the nozzle. Consequently, voids resulting from extrusion and lofting (swelling of the plastificate after extrusion) are neglected. The second-order FOT (cf. Eq. (1)) is approximated by the weighted summation of artificial unit FV $\boldsymbol{p}$ for each cell:

$$\boldsymbol{A} = \frac{1}{\sum_k w_k} \sum_k \boldsymbol{p}_k \otimes \boldsymbol{p}_k w_k \,. \tag{3}$$

w denotes the k-th weight function of the individual FV. The FV correspond to the tangent and normal of the ellipses, respectively. Three ellipses are constructed with respect to the position of the two extruder screws and the center of the plastificate's cross-section (cf. Figure 1). We choose the semi-major (horizontal) and semi-minor (vertical) axis (a, b) according to the plastificate's width and height to (width/4, height/2) and (width/2, height/2), respectively. The tangent FV $\boldsymbol{p}^c_{\mathrm{t},1}$ and $\boldsymbol{p}^c_{\mathrm{t},2}$ of the lateral ellipses approximate the swirl-like fiber orientation. The notation $(\cdot)^c$ denotes the c-th cell. The tangent FV $\boldsymbol{p}^c_{\mathrm{t},3}$ of the center ellipse increases the degree of orientation in the circumferential direction in the outer area. The degree of isotropy is adjusted by the normal FV $\boldsymbol{p}^c_{\mathrm{n},1}$ and $\boldsymbol{p}^c_{\mathrm{n},2}$ of the lateral ellipses.

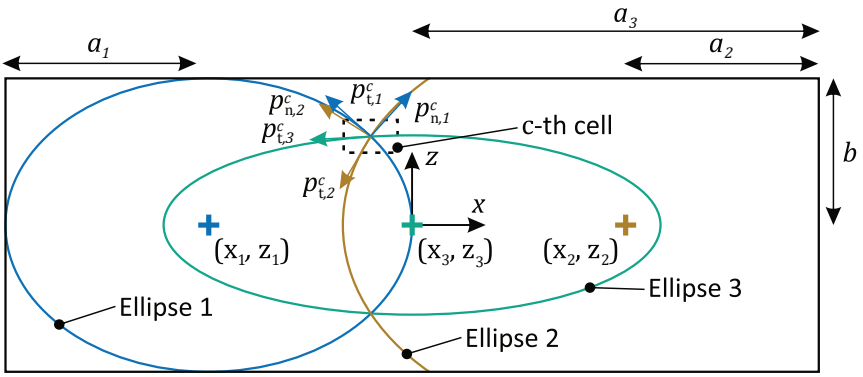

Figure 1. Geometric construction of artificial FV based on the tangent and normal of the three ellipses for the c-th cell. (x_k, z_k) denote the respective ellipse centers.

In the following, it is assumed that the coordinate system is in the middle of the plastificate's cross-section and that the y-axis corresponds to the extrusion direction, see Figure 1. The weight functions for the tangent FV $\boldsymbol{p}^c_{\mathrm{t},1}$ and $\boldsymbol{p}^c_{\mathrm{t},2}$ are defined as:

$$w_{\mathrm{t},1} = \frac{(d_1+d_2)}{d_1}\,,\quad w_{\mathrm{t},2} = \frac{(d_1+d_2)}{d_2}, \tag{4}$$

with d_1 and d_2 being the Euclidean distance from the cell center to the respective ellipse center.

  doi:10.5075/epfl-298799_978-2-9701614-0-0

The weight function of the FV $\boldsymbol{p}_{\mathrm{t},3}^{c}$ are defined by scaling the latter weight functions depending on the cell coordinates:

$$w_{\mathrm{t},3} = \begin{cases} w_{\mathrm{t},1}\,\mathrm{argmax}\left(\frac{|z|}{b}, \frac{|x|}{a_3}\right)^4, & x \leq 0 \\ w_{\mathrm{t},2}\,\mathrm{argmax}\left(\frac{|z|}{b}, \frac{|x|}{a_3}\right)^4, & x > 0 \end{cases}. \tag{5}$$

The weight functions of the normal FV $\boldsymbol{p}_{\mathrm{n},1}^{c}$ and $\boldsymbol{p}_{\mathrm{n},2}^{c}$ are chosen to increase the degree of isotropy in the area between the extruder screw. The latter are defined as:

$$w_{\mathrm{n},i} = w_{\mathrm{t},i}\,\mathrm{argmin}\left(1 - \frac{|z|}{\mathrm{b}}, 1 - \frac{|x|}{\mathrm{a}_3}\right)^2, \quad i = 1, 2. \tag{6}$$

So far, only planar FOT were defined in the (x, z)-plane. To account for the orientation in the extrusion direction, the weighted summation of the in-plane FOT and a unidirectional FOS with $A_{yy} = 1$ are calculated, with the ratio of the respective weight factors defining the degree of orientation in the extrusion direction. The strong anisotropy in the boundary layer of the plastificate was considered by assigning a unidirectional orientation state in the extrusion direction (A_{yy} = 1) to the outermost cells. The approximation of the artificial FOT is independent of the extrusion direction, which is why all cells with identical (x, z)-coordinates have identical FOT.

2.2 Compression molding simulation

The numerical investigation was conducted on a (400 x 400 x 3) mm plate tool. The (75 x 200 x 35) mm plastificate was placed in the center of the mold. The plate was meshed with 20 elements in the thickness direction, corresponding to a total of 4,156,197 tetrahedrons. The compression molding simulations were conducted using Moldflow 2021.1. The used CF/PA6 material "OnForce™ LFT-NN40LCF001" was given in the Moldflow material database. We used the RSC [11] model to account for the reorientation of fibers. To elaborate the influence of the initial FOS for different flow regimes, we conducted simulations with different values for the retarding rate κ and the interaction coefficient C_{i}. Namely, κ = 0 and C_{i} = 0, reducing the model to Jeffery's equation [12], κ = 0.1 and C_{i} = 0, and κ = C_{i} = 0.1. We ran simulations with those parameter sets for the following initial FOS: artificial (plastificate generator), planar-isotropic (A_{xx} = A_{yy} = 0.5) and isotropic (A_{xx} = A_{yy} = A_{zz} = 1/3). The weight factors for the extrusion direction of the artificial FOT were chosen so that A_{yy} = 0.3, which corresponds to the averaged A_{yy} of the evaluated µCT volumes.

2.3 Fiber orientation measurement

The Zeiss Metrotom 800 (cone-beam) µCT system with the flat panel detector PaxScan2520V with (1536 x 1920) pixels was used to scan a section of the plastificate. The scan resolution was 73 µm/voxel, which corresponds to the maximal resolution. The resulting volumetric images were reconstructed applying the Feldkamp cone-beam algorithm [13] and the Shepp-Logan noise reduction filter. Subsequently, the reconstructed scans were processed in VG Studio Max 3.4.2. A grid of 36 (3.33 x 3.33 x 3.33) mm cubes was superimposed around the left swirl. Each cell was evaluated individually in the further process of the FOT determination. If necessary,

  doi:10.5075/epfl-298799_978-2-9701614-0-0

brightness and contrast were adjusted within the software ImageJ (FIJI). In addition, the individual gray value threshold was determined for each cell using Otsu's method [14]. To determine the FOT from the scan data, the method introduced by Pinter et al. [7] was used. The algorithm makes use of the structure tensor:

$$\boldsymbol{S} = \begin{bmatrix} \left(\frac{\delta I}{\delta x}\right)^2 & \frac{\delta I}{\delta x}\frac{\delta I}{\delta y} & \frac{\delta I}{\delta x}\frac{\delta I}{\delta z} \\ \frac{\delta I}{\delta y}\frac{\delta I}{\delta x} & \left(\frac{\delta I}{\delta y}\right)^2 & \frac{\delta I}{\delta y}\frac{\delta I}{\delta z} \\ \frac{\delta I}{\delta z}\frac{\delta I}{\delta x} & \frac{\delta I}{\delta z}\frac{\delta I}{\delta y} & \left(\frac{\delta I}{\delta z}\right)^2 \end{bmatrix}, \tag{2}$$

with I being a discrete function describing the grey-value intensity of the reconstructed image. The structure tensor calculation is combined with a Gaussian blur of a width of σ = 0.2 voxels and a mask size of 2 voxels. As a result, the second-order FOT was obtained for each cell.

3. Results

Figure 2 shows the estimated FOT of µCT volumes around the left extruder screw and the FOT of the plastificate generator of the right half of the plastificate in the (x, z)-plane perpendicular to the extrusion direction represented by tensor glyphs [15]. Unidirectional FOT, e.g., A_{yy} = 1, are represented as lines by tensor glyphs and are therefore not visible in Figure 2 (concerns boundary layer of artificial FOS). The FOT of the µCT volumes as well as the artificial ones show a swirl-like pattern, as reported by [2]. However, individual FOT from µCT volumes have strongly deviating orientation states compared to their adjacent cells. As expected, the artificial FOT map the averaged expected fiber orientation of the investigated extrusion process. The latter tensors show a significant alignment of the fibers in the circumferential direction in the outer area, which is to be expected due to the concurrent extruder screws. The lateral artificial FOT exhibit a stronger alignment than near the top and bottom, which is caused by the chosen weight functions.

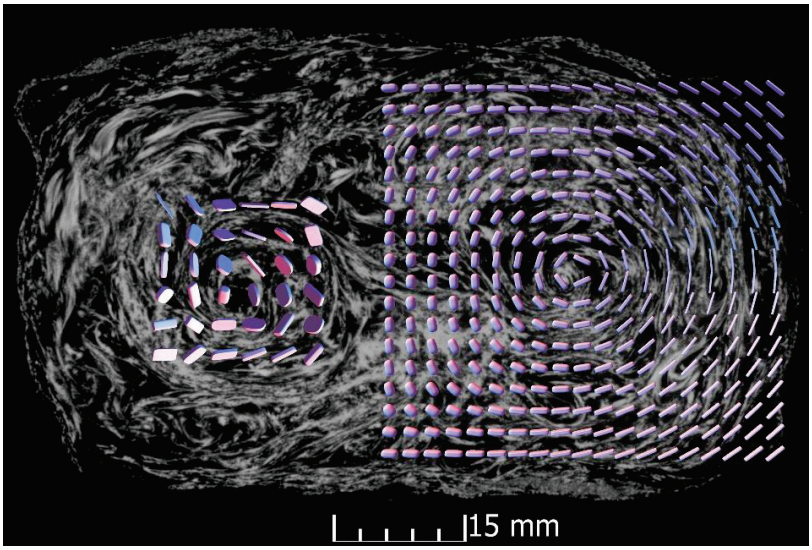

Figure 2. FOT from µCT images (left) and from the plastificate generator (right) represented by tensor glyphs [15] in front of a µCT image of the evaluated volume.

  doi:10.5075/epfl-298799_978-2-9701614-0-0

The fiber orientation results for A_{xx} and A_{yy} of the compression molding simulations of the different initial FOS are shown in Figure 3. The A_{zz} component is omitted since it is given by tr(A_{ii}) = 1. The evaluation was carried out at Position A close to the plastificate's initial position and Position B near the end of the flow. The results using Jeffery's equation show significant fiber alignment in the flow direction, however, the influence of the initial FOS is pronounced. The introduction of the retarding rate κ reduces the rate of reorientation. The influence of the initial FOS is insignificant when using a high interaction coefficient C_i. Further, the fiber orientation of the latter is more random in the (x, y)-plane.

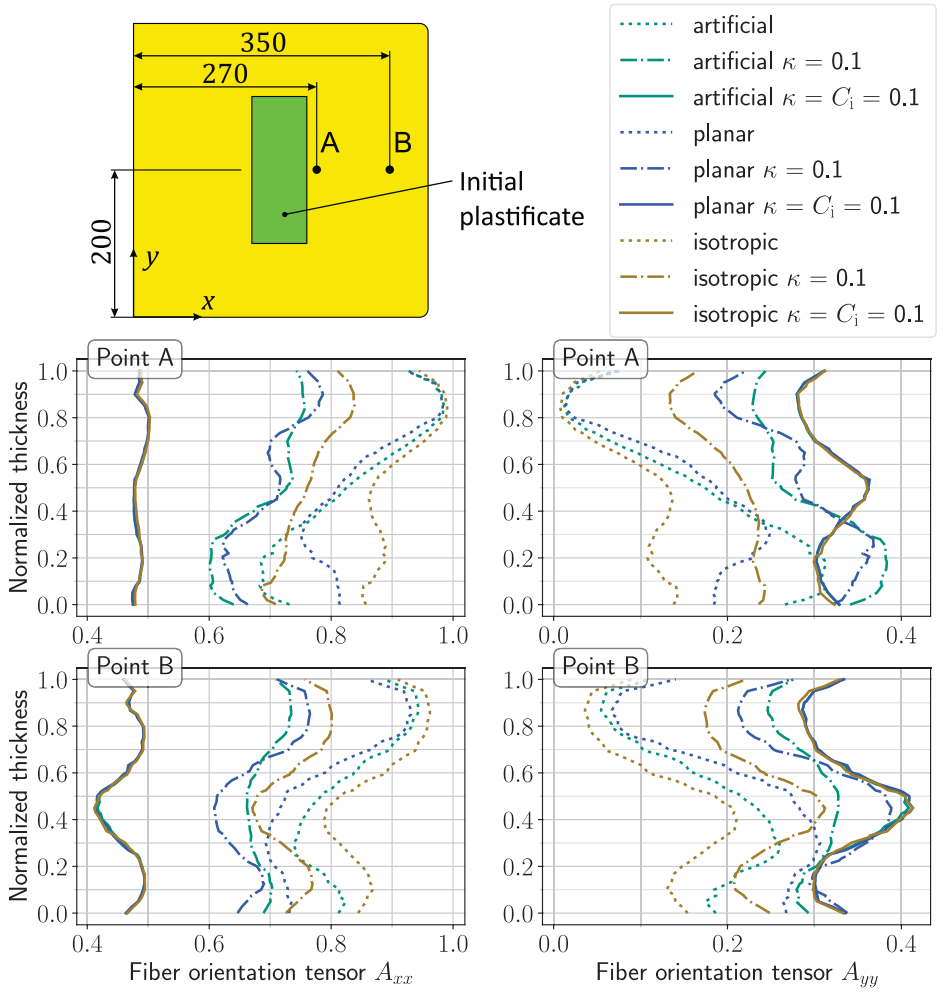

Figure 3. Comparison of FOT components A_{xx} and A_{yy} at locations A (upper graphs) and B (lower graphs) through the thickness for different initial FOS and RSC model parameters.

4. Discussion

There are limits to the comparison of the fiber orientation state determined from the µCT volumes and the artificially generated one. While the plastificate generator outputs deterministic FOT, the physical plastificate is subjected to strong statistical variations, e.g., voids, presence and distribution of fiber bundles (relevant for low µCT resolution) and fiber breakage. This leads to strong local deviations from the averaged expected fiber orientation, caused by too few voxels per cell (compare for example the FOT in the upper left tensor glyph in Figure 2 on

  doi:10.5075/epfl-298799_978-2-9701614-0-0

the left), not to mention the resolution problem. If the cell size is increased, however, the FOS tends to be more isotropic and therefore not reasonable. The same applies to the idea of averaging orientation tensors, e.g., in extrusion direction, to reduce the statistical variations. On the one hand, this touches on the well-known problem of finding representative volume elements, which have often been converted into statistical volume elements for fiber-reinforced plastics. On the other hand, this depicts the problem to correctly interpolate or average tensors for larger volumes and areas. The question of a suitable error measure also arises for the direct comparison of tensors, since neither a direct component comparison nor, e.g., the use of the Frobenius norm has proved particularly useful. Furthermore, the large number of voids in the plastificate complicate the identification of fiber bundles, because the gray value drop between CF and thermoplastic is much smaller compared to the drop to air. This effect does not apply to finished parts as the air escapes during molding. Therefore, the estimated FOT from µCT images of the plastificate can only be considered correct under the condition of the uniform behavior of the fibers to the matrix in the flow. Consequently, the comparison of FOT from µCT volumes of the plastificate (independent of the scan resolution) and the plastificate generator is not suitable for validation. Rather, the validation must be based on the comparison of a compression molded part's final virtual and physical fiber orientation.

The results of the compression molding simulations illustrate the influence of the initial FOS for different flow regimes. Jeffery's equation retains the information of the initial FOS most, as the fiber reorientation only depends on the rotation and rate of deformation of the surrounding thermoplastic. On the other hand, the influence of the initial FOS is negligible for high interaction coefficients C_i as the state of equilibrium is more random and therefore reached faster (compare results for C_i = 0.1 in Figure 3). However, a high value of this coefficient does not approximate the physical process as the fibers exhibit a significant alignment in the flow direction dependent on the flow path. Consequently, the interaction coefficient must be sufficiently small so that the resulting state of equilibrium has a strong orientation in the flow direction.

5. Conclusion

In this work a novel approach based on the construction of artificial fiber vectors (FV) from ellipses is developed to consider the initial FOS of an LFT plastificate in compression molding simulation. Qualitative comparison with µCT images shows that the proposed FOS generator maps the expected averaged FOS of the physical plastificate. However, quantitative comparison with FOS from µCT volumes depict several challenges, which impedes validation, especially for CF. The results of the compression molding simulations show a non-negligible influence of the initial FOS for long fiber reinforced polymers. Therefore, the approach must be validated based on a physical part's final fiber orientation at sample locations.

6. Contributions

LS: Conceptualization, Methodology, Software, Writing – original draft. **JB**: Investigation, Resources, Writing - review & editing. **KH**: Investigation, Resources. **NM**: Conceptualization, Writing – review & editing. **LK**: Supervision, Writing - review & editing.

7. Acknowledgements

The research documented in this manuscript has been funded by the German Research Foundation (DFG) within the International Research Training Group "Integrated engineering of

  doi:10.5075/epfl-298799_978-2-9701614-0-0

continuous-discontinuous long fiber reinforced polymer structures" (IRTG 2078). The support by the German Research Foundation (DFG) is gratefully acknowledged. Furthermore, the authors would also like to thank the Fraunhofer ICT for their support by providing the LFT plastificates, which were manufactured under the project leadership of Christoph Schelleis.

8. References

1. Ning H, Lu N, Hassen AA, Chawla K, Selim M, Pillay S. A review of Long fibre thermoplastic (LFT) composites. International Materials Reviews 2020; 65:164-188.
2. Perez C, Osswald T, Goris S. Study on the fiber properties of a LFT strand. 2013.
3. Folgar F, Tucker C. Orientation Behavior of Fibers in Concentrated Suspensions. Journal of Reinforced Plastics and Composites 1984; 3(2):98-119.
4. Advani S, Tucker C. The Use of Tensors to Describe and Predict Fiber Orientation in Short Fiber Composites. Journal of Rheology 1987; 31(8):751-784.
5. Gandhi U, Sebastian DB, Kunc V, Song Y. Method to measure orientation of discontinuous fiber embedded in the polymer matrix from computerized tomography scan data. Journal of Thermoplastic Composite Materials 2016; 29(12):1696-1709.
6. Schladitz K, Büter A, Godehardt M, Wirjadi O, Fleckenstein J, Gerster T, Hassler U, Jaschek K, Maisl M, Maisl U, Mohr S, Netzelmann U, Potyra T, Steinhauser MO. Non-destructive characterization of fiber orientation in reinforced SMC as input for simulation based design. Composite Structures 2017; 160:195-203.
7. Pinter P, Dietrich S, Bertram B, Kehrer L, Elsner P, Weidenmann KA. Comparison and error estimation of 3D fibre orientation analysis of computed tomography image data for fibre reinforced composites. NDT & E International 2018; 95: 26–35.
8. Jördens C, Scheller M, Wietzke S, Romeike D, Jansen C, Zentgraf T, Wiesauer K, Reisecker V, Koch M. Terahertz spectroscopy to study the orientation of glass fibres in reinforced plastics. Composites Science and Technology 2010; 70(3):472-477.
9. Song Y, Gandhi U, Pérez C, Osswald T, Vallury S, Yang A. Method to account for the fiber orientation of the initial charge on the fiber orientation of finished part in compression molding simulation. Composites Part A 2017; 100:244-254.
10. Song Y, Gandhi U, Sekito T, Vaidya UK, Vallury S, Yang A, Osswald T. CAE method for compression molding of carbon fiber-reinforced thermoplastic composite using bulk materials. Composites Part A 2018; 114:388-397.
11. Wang J, O'Gara JF, Tucker CL. An objective model for slow orientation kinetics in concentrated fiber suspensions: Theory and rheological evidence. Journal of Rheology 2008; 52(5):1179-1200.
12. Jeffery GB. The Motion of Ellipsoidal Particles Immersed in a Viscous Fluid. Proceedings of the Royal Society of London. Series A, Containing Papers of a Mathematical and Physical Character 1922; 102:161-179.
13. Feldkamp LA, Davis LC, Kress JW. Practical cone-beam algorithm. Journal of the Optical Society of America A 1984; 1(6): 612–9.
14. Otsu N. A Threshold Selection Method from Gray-Level Histograms. IEEE Trans. Syst., Man, Cybern. 1979; 9(1): 62–6. https://doi.org/10.1109/TSMC.1979.4310076.
15. Schultz T, Kindlmann GL. Superquadric glyphs for symmetric second-order tensors. IEEE Trans Vis Comput Graph 2010; 16(6): 1595–604.

